International Communications in Heat and Mass Transfer 35 (2008) 492–502

Entropy generation for natural convection by heated partitions in a cavity

M. Famouri[1] and K. Hooman[2]

[1] Mechanical Engineering Faculty, Noushirvani Institute of Technology, Babol, Iran

[2]School of Engineering, The University of Queensland, Brisbane, Australia

Abstract

Entropy generation for natural convection in a partitioned cavity, with adiabatic horizontal and isothermally cooled vertical walls, is studied numerically by both a FORTRAN code and the commercially available CFD-ACE software. Effects of the Rayleigh number, the position of the heated partition, and the dimensionless temperature difference on the local and average entropy generation rate are investigated. Proper scale analysis of the problem showed that, while fluid friction term has nearly no contribution to entropy production, the heat transfer irreversibility increases monotonically with the Nusselt number and the dimensionless temperature difference.

Keywords: Natural convection, entropy generation, partitioned space, numerical

Nomenclature

Be	Bejan number
c_P	specific heat at constant pressure
FFI	fluid friction irreversibility
Ge	Gebhart number
H	cavity height
HTI	heat transfer irreversibility
k	fluid thermal conductivity
*Ns**	normalized *Ns*
Ns	dimensionless entropy generation number
Nu	Nusselt number
*P**	pressure
p	dimensionless pressure
Pr	Prandtl number, $Pr=\mu c_p/k$
q''	total inlet or outlet wall heat flux
Ra	Rayleigh number, $Ra=g\beta H^3(T_h-T_c)/(\alpha\upsilon)$

$\dot{S}_{gen}$ volumetric entropy generation rate

T^* absolute temperature

T_c the cold wall temperature

T_h the plate temperature

(u^*,v^*) (x^*,y^*) velocity

u,v $(u^*,v^*)\alpha/H$

(x^*,y^*) Cartesian coordinates

(x,y) $(x^*,y^*)/H$

Greek symbols

θ dimensionless temperature, $(T^*-T_c)/(T_h-T_c)$

μ fluid viscosity

ρ fluid density

ψ dimensionless stream function

ϕ dimensionless viscous dissipation function, $\phi = H^4\phi^*/\alpha^2$

ϕ^* viscous dissipation function

ω dimensionless vorticity

Ω dimensionless temperature difference $(T_h-T_c)/T_c$

1. Introduction

Free convection in partitioned spaces is of particular interest in many engineering applications as noted by [1-7]. Hence, a great deal of information is available on heat and fluid flow through such enclosures as reviewed by Bejan [8]. Using a Laser Doppler Anemometer, turbulent natural convection of air in a partitioned cavity with differentially heated vertical and conducting horizontal walls was studied in [3]. On the other hand, dealing with laminar free convection in a differentially heated, partitioned, square cavity filled with a heat-generating fluid, Oztop and Bilgen [6] concluded that depending on the ratio of the internal/external Rayleigh number, there are two distinct regimes. Also they noted that the flow field will be adapted due to the presence of partial dividers while heat transfer is expected to reduce when this *Ra* ratio is from 10 to 100. Prior to that, Bilgen and Oztop [7] have performed a numerical study on inclined partially open square cavity to observe that heat transfer can be maximized or minimized by selecting appropriate parameters, namely aperture size, position and inclination angle at a given *Ra*. Oztop et al. [9] studied the effect

of the position and the aspect ratio of a thin heated plate on free convection in a cavity to find that *Nu* increases with *Ra* and concluded that the enhancement is more pronounced for vertical plate.

Also available in the literature is an extensive amount of work devoted to optimal design of such systems. For example Bilgen [10] studied the effects of a thin fin attached to the cavity wall to realize that *Nu* increases/decreases with *Ra*/the fin length and relative conductivity ratio. Interestingly, he noted that there is always an optimum fin position, which is often at the center or near center of the cavity, which minimizes natural convection heat transfer. Recently, Bar-Cohen et al. [4] determined the most favorable fin and channel aspect ratios for plate and pin fin arrays, the allocation of available energy between fabrication and operation, and the selection of fin material, for both natural and forced convection air-cooled heat sinks.

On the other hand, when it comes to seek optimum design features for a system, Entropy Generation Minimization (EGM), as introduced by Bejan [11], serves as a popular approach. This method has already been extensively applied to forced [12-16] and free convection [17-25] problems, to name a few. However, for the problem considered here there is no solution reported in the literature, to the best knowledge of the authors. This paper presents numerical solution for heat and fluid flow of a fluid in such cavity similar to [9]. Based on our results for the first law (of thermodynamics), second law aspects of the problem are then investigated. Two numerical solvers are cross-validated here being our FORTRAN code and the commercially available software CFD-ACE.

The considered physical geometry with related parameters and coordinates are shown in Fig. 1. The plate, of thickness 0.05*H*, is supposed to be isothermal at higher temperature than two vertical isothermal walls while the top and bottom walls are insulated.

2. Governing Equations

2.1. Heat and Fluid Flow Analysis

The dimensionless vorticity transport equation is

$$u.\nabla\omega = \mathrm{Pr}(\nabla^2\omega - Ra\frac{\partial\theta}{\partial x}) \tag{1}$$

where the vorticity directed in *z* direction is defined as

$$\omega = -\nabla^2\psi\,. \tag{2}$$

In the above equation the dimensionless stream-function is defined as

$$u = \frac{\partial \psi}{\partial y}, \qquad \mathrm{v} = -\frac{\partial \psi}{\partial x}. \tag{3-a,b}$$

The thermal energy equation now takes the following form

$$u.\nabla\theta = \nabla^2\theta\,. \tag{4}$$

The average Nusselt number, the ratio of actual heat transfer to pure conduction, is defined as

$$Nu = \frac{1}{4}\int_0^1 \left(\frac{\partial\theta(0,y)}{\partial x} + \frac{\partial\theta(1,y)}{\partial x}\right)dy. \tag{5}$$

Note that the Nusselt number defined by Oztop et al. [9] is twice our *Nu*. Consequently, for low *Ra* cases, where heat is transferred mainly due to conduction and one expects near-unity values for *Nu*, they came up with *Nu*~2. However, as it can be observed later, for low *Ra* values, based on our definition, *Nu*→1 in our work.

The problem is now to solve Eqs. (1-6) subject to no-slip boundary condition on the walls, i.e. *u*=*v*=0, and the following thermal boundary conditions

$$\begin{aligned} &\frac{\partial\theta}{\partial y} = 0; \ \text{horizontal walls,} \\ &\theta = 0; \quad \text{vertical walls,} \\ &\theta = 1; \quad \text{plate.} \end{aligned} \tag{6}$$

2.2. Second Law aspects of the problem

According to Bejan [11], one can find the volumetric entropy generation rate as

$$\dot{S}_{gen} = HTI + FFI\,, \tag{7}$$

where *HTI* is the irreversibility due to heat transfer in the direction of finite temperature gradients and *FFI* is the contribution of fluid friction irreversibility to the total generated entropy.

In terms of the primitive variables, *HTI* and *FFI* become

$$HTI = k(\nabla T^*.\nabla T^*)/T^{*2}, \qquad FFI = \mu\phi^*/T^*. \tag{8-a,b}$$

One can also define the Bejan number, *Be*, as

$$Be = HTI/(HTI+FFI). \tag{9}$$

Note that a *Be* value more/less than 0.5 shows that the contribution of *HTI* to the total entropy generation is higher/less than that of *FFI*. The limiting value of *Be*=1 shows that the only active entropy generation mechanism is *HTI* while *Be*=0 represents no *HTI* contribution.

The dimensionless form of entropy generation rate, *Ns*, is defined as

$$Ns = (H/\Omega)^2 \dot{S}_{gen}/k, \tag{10}$$

one finds that

$$Ns = \frac{(\frac{\partial\theta}{\partial x})^2 + (\frac{\partial\theta}{\partial y})^2}{\Omega^2\left(\Omega^{-1}+\theta\right)^2} + \frac{Ge\phi}{Ra\Omega^2\left(\Omega^{-1}+\theta\right)}, \tag{11}$$

where the dimensionless temperature difference is defined as

$$\Omega=(T_h-T_c)/T_c \tag{12}$$

The dimensionless viscous dissipation function, addressed in Eq. (11), takes the following form

$$\phi = 2(\frac{\partial u}{\partial x})^2 + 2(\frac{\partial v}{\partial y})^2 + (\frac{\partial v}{\partial x} + \frac{\partial u}{\partial y})^2 \tag{13}$$

One easily verifies that, as both Ω and θ can put on values smaller than unity, one cannot neglect any of them in favor of the other as noted by Hooman and Ejlali [26] for a forced convection problem. Keep in mind that Ω can be $O(1)$ for special cases. Hence, one should be very careful when one simply neglects either Ω^{-1} or θ in the denominator of Eq. (11) by Ω.

Here, *Ge* is the Gebhart number which is defined as

$$Ge = g\beta H/c_P, \tag{14}$$

and throughout this work $Ge=10^{-5}$ to be a real choice for most of engineering applications. In the light of Nield [27, 28] one knows that the proper dimensionless number to show the effects of viscous dissipation in a free convection problem in a cavity, filled with or without a porous insert, is the Gebhart number which, interestingly, does not contain viscosity. This was also highlighted by Hooman [29]. Unlike the previous findings of Dagtekin et al. [30], proper scaling shows that with a fixed *Ge* value *FFI* decreases with *Ra*. Interestingly, both *HTI* and *Ns* increase with *Ra* and this will be elaborated on in the forgoing discussion.

It should also be noted that there are certain cases where viscous dissipation effects are not important in the thermal energy equation but can be significant when it comes to study second law aspects of a convection problem as outlined by Bejan [11] or Hooman et al. [31]. The local and average values of *Be* are found to convey little information as they are very close to unity, hence, we did not present any graph or contour for *Be*.

Average *Ns* is denoted by $<Ns>$, where the angle brackets show an average taken over the area, as

$$<Ns> = \int_A NsdA/A \tag{15}$$

where, based on the dimensionless cavity size (1x1 box) shown in Fig. 1, Eq. 15 reads

$$<Ns> = \int_0^1\int_0^1 Nsdxdy\,. \tag{16}$$

Selecting the fluid, trapped between the heated plate and the cavity, as the thermodynamic system, one observes that the amount of heat entered through the heated plate is equal to the one transferred to the surroundings via the isothermal walls. Moreover, one notes that the total volumetric entropy generation rate is obtainable as

$$<\dot{S}_{gen}>=\frac{q''}{H}(\frac{1}{T_c}-\frac{1}{T_H}) \quad (17)$$

where, in terms of *Nu*, it reads

$$<\dot{S}_{gen}>=4Nu\frac{k}{H^2}\frac{\Omega^2}{1+\Omega} \quad (18\text{-a})$$

Applying perturbation techniques for small values of Ω, say Ω<<1, one has

$$<\dot{S}_{gen}>\approx 4Nu\Omega^2(1-\Omega)k/H^2 \quad (18\text{-b})$$

The dimensionless entropy generation number can be obtained as

$$<Ns>=4Nu/(1+\Omega) \quad (19)$$

This analytically obtained equation is used for validation purpose as manifested in our Table 1.

3. Numerical Details

Numerical solutions to the governing equations are obtained by finite difference methods, using the Gauss-Seidel technique. The governing equations are discretized by applying second-order accurate central difference schemes similar to [32]. Details of the vorticity-stream-function method, and applied boundary conditions may be found in [33] and are not repeated here.

All runs were performed on a 101x101 grid with *Ra* limited to 10^5, *Pr*=0.7, and $h_3=0.5H$. Grid independence was verified by running different combinations of *Ra* and h_1 ($h_i=h_i*/H$) on three different grids 81x81, 101x101 and 121x121 and observing less than 1% difference between results obtained on smaller grids. The convergence criterion (maximum relative error in the values of the dependent variables between two successive iterations) in all runs was set at 10^{-5}.

The above procedure was done for the validation of the FORTRAN code and repeated for the other solver being CFD-ACE where we used triangular mesh system with a transition factor 1.1 and the minimum cell size of 10^{-5}. We then changed the maximum cell size from 0.1 to 0.01 to see that the results, based on these two different grids, are effectively the same.

4. Results and Discussions

Figs. 2-4 shows contours of θ, ψ, and *Ns** (*Ns**=*Ns*/Ns_{max}) for *Ra*=10^3, 10^4, and 10^5, when the position of the partition changes along the vertical direction with h_1=0.75, 0.5, and 0.25, respectively. It is clear that increasing *Ra*, there is more vigorous mixing and hence there are severe

temperature gradients at the top (left and right) corners. This is also confirmed by *Ns** contours. As the fluid flow and heat transfer aspects of this problem were previously studied by Oztop et al. [9], we will skip the details and focus on the second law aspects of the problem. As seen, for any arrangement of the partition, the active sites of entropy production are regions close to the heated plate where the highest heat flux can be detected due to the presence of the heat source, i.e. the plate. It is also clear that with high *Ra* values the top corners are acting as active sites of entropy generation. Discussing the heatline distribution for a natural convection problem, Bejan [8] interpreted it as 'heat rises'. Similar argument was put forward by Hooman and Gurgenci [34] for a lateral heating free convection problem. Before moving to the global aspects of the problem, it should be noted that as the results of the two solvers were very close (the difference was in the fourth figure) Fig. 5 is designed to indicate a sample of our calculations using CFD-ACE software, for h_1 =0.5 with $Ra=10^3$, 10^4 and 10^5 for a qualitative comparison.

Fig. 6 shows *Nu* and ψ_{max} for different *Ra* and h_1 values. It can be concluded that for $Ra=10^3$ the heat transfer mechanism is effectively a pure conduction one as *Nu* is very close to unity. Commensurate with that are very small values of $\psi_{max.}$ However, for $Ra>10^4$ convective flow patterns are strong enough to lead to *Nu*>1 and this can be called, to the first approximation, the critical value beyond which convective heat transfer enhances with an increase in *Ra*. Moving the plate from the bottom wall to the top one, ψ_{max} decreases as the flow region is restricted to smaller area sandwiched between the plate and the top wall. The Nusselt number acts more or less the same while with h_1=0 the problem tends to the classical Bénard problem where for $h_1=1$ there is no flow and the heat is transferred by pure conduction. An interesting observation is the interaction between convective flow strength and the position of the heated plate. As seen, ψ_{max} decreases monotonically with h_1 while *Nu* puts on higher values for h_1=0.5 compared to that of h_1=0.25. It can be explained as follows. With h_1=0.5, the flow and temperature distribution patterns are symmetrical with respect to the plate for low *Ra* values as heat is mostly transferred due to conduction. There are also diagonal symmetry lines for the streamlines on top of vertical and horizontal ones. This means that for such a case, there are two adiabatic lines while with other values of h_1, there exists just a vertical one. Hence the heat transfer in the regions in between these lines increase to make up for the fact that there is no heat transfer along such lines. This is similar to the discussion proposed by Hooman et al. [31] in their study of fully developed forced convection in a porous duct of square cross-section. However, increasing *Ra* the effect of symmetry becomes less important as the two curves, for h_1=0.25 and 0.5, merge together with $Ra=10^5$. On the other hand, the slope of *Nu*-*Ra* curve implies that for higher *Ra* values *Nu* would show similar trend as that of ψ_{max}, i.e. decrease with h_1.

According to Fig. 7, an increase in Ω decreases/increases $<Ns>$/ $<\acute{S}_{gen}>$. This fact is in line with the predictions of our Eqns. (18-19). This also makes physical sense since, as $\Omega=T_h/T_c-1$, higher values of Ω imply a greater temperature difference (leading to higher heat transfer rates) and consequently boosted *HTI* values. The decrease in $<Ns>$ should not be interpreted as a decrease in the total entropy generation since, as noted earlier, one has $\acute{S}_{gen}=Nsk(\Omega/H)^2=4Nuk(\Omega/H)^2/(1+\Omega)$. Another point worthy of comment is that $<Ns>$ values for $Ra=10^5$ are notably high; however, among them the case $h_1=0.75$ remains very close to those of lower *Ra* values as in this case effective circulation zone is restricted to the top quarter of the cavity and the regions beneath the plate are effectively transferring heat due to conduction. This point is also valid for $h_1=0.75$ and $Ra=10^4$ compared to $h_1=0.5$ and $Ra=10^3$.

5. Conclusion

Numerical simulation of free convection in a partitioned cavity, with special attention being paid to entropy generation, is reported. Effects of the Rayleigh number, the position of the heated partition, and the dimensionless temperature difference on the local and average entropy generation rate are investigated. It was theoretically indicated that the average entropy production rate increases with *Nu* and Ω. It was also shown and emphasized that with a fixed *Ge* value, *FFI* is an inverse-linear function of *Ra* while numerical results showed that for most cases, with a fixed value for h_1, *HTI* increases with *Ra* and so does the total generated entropy.

Acknowledgment

The second author acknowledges the support provided by The University of Queensland in terms of UQILAS, Endeavor IPRS, and School Scholarship.

References,

[1] Bar-Cohen A, Iyengar M. Least-energy optimization of air-cooled heat sinks for sustainable development. IEEE Trans Compon Packaging Technol 2003;26(1):16-25.
[2] Naphon P. On the performance and entropy generation of the double-pass solar air heater with longitudinal fins. Renew Energy 2005;30(9):1345-57.
[3] Ampofo F. Turbulent natural convection of air in a non-partitioned or partitioned cavity with differentially heated vertical and conducting horizontal walls. Exp Therm Fluid Sci 2005;29(2):137-57.
[4] Bar-Cohen A, Bahadur R, Iyengar M. Least-energy optimization of air-cooled heat sinks for sustainability-theory, geometry and material selection. Energy 2006;31(5):579-619.

[5] Merrikh AA, Lage JL, Mohamad AA. Natural convection in nonhomogeneous heat-generating media: Comparison of continuum and porous-continuum models. J Porous Media 2005;8(2):149-63.
[6] Oztop H, Bilgen E. Natural convection in differentially heated and partially divided square cavities with internal heat generation. Int J Heat Fluid Flow 2006;27(3):466-75.
[7] Bilgen E, Oztop H. Natural convection heat transfer in partially open inclined square cavities. Int J Heat Mass Transf 2005;48(8):1470-79.
[8] Bejan A. Convection heat transfer Hoboken, N.J.: Wiley, 2004.
[9] Oztop HF, Dagtekin I, Bahloul A. Comparison of position of a heated thin plate located in a cavity for natural convection. International Communications in Heat and Mass Transfer 2004;31(1):121-32.
[10] Bilgen E. Natural convection in cavities with a thin fin on the hot wall. Int J Heat Mass Transf 2005;48(17):3493-505.
[11] Bejan A. Entropy generation through heat and fluid flow. New York: Wiley, 1982.
[12] Hooman K, Ejlali A. Entropy generation for forced convection in a porous saturated circular tube with uniform wall temperature. International Communications in Heat and Mass Transfer 2007;34(4):408-19.
[13] Hooman K, Gurgenci H. Effects of temperature-dependent viscosity variation on entropy generation, heat and fluid flow through a porous-saturated duct of rectangular cross-section. Appl Math Mech-Engl Ed 2007;28(1):69-78.
[14] Hooman K. Entropy-energy analysis of forced convection in a porous-saturated circular tube considering temperature-dependent viscosity effects. Int J Exergy 2006;3(4):436-51.
[15] Hooman K, Haji-Sheikh A. Analysis of heat transfer and entropy generation for a thermally developing Brinkman-Brinkman forced convection problem in a rectangular duct with isoflux walls. Int J Heat Mass Transf 2007;50:4180-94.
[16] Hooman K. Entropy generation for microscale forced convection: effects of different thermal boundary conditions, velocity slip, temperature jump, viscous dissipation, and duct geometry. International Communications in Heat and Mass Transfer 2007;34:945-57.
[17] Baytas AC. Entropy generation for natural convection in an inclined porous cavity. Int J Heat Mass Transf 2000;43(12):2089-99.
[18] Baytas AC. Optimization in an inclined enclosure for minimum entropy generation in natural convection. Journal of Non-Equilibrium Thermodynamics 1997;22(2):145-55.
[19] Slimi K. Entropy generation for unsteady natural convection and radiation within a tilted saturated porous channel. Int J Exergy 2006;3(2):174-90.
[20] Abu-Hijleh BAK. Optimized use of baffles for reduced natural convection heat transfer from a horizontal cylinder. Int J Therm Sci 2003;42(11):1061-71.
[21] Ibanez G, Cuevas S, de Haro ML. Minimization of entropy generation by asymmetric convective cooling. Int J Heat Mass Transf 2003;46(8):1321-28.
[22] Erbay LB, Altaç Z, Sülüs B. An Analysis of The Entropy Generation in a Square Enclosure Entropy 2003;5(5):496-505
[23] Abu-Hijleh BAK. Optimization of natural convection heat transfer from a cylinder with high conductivity fins. Numer Heat Tranf A-Appl 2003;43(1):65-82.
[24] Adeyinka OB, Naterer GF. Apparent entropy production difference with heat and fluid flow irreversibilities. Numer Heat Tranf B-Fundam 2002;42(5):411-36.

[25] Abu-Hijleh B. Natural convection and entropy generation from a cylinder with high conductivity fins. Numer Heat Tranf A-Appl 2001;39(4):405-32.
[26] Hooman K, Ejlali A. Second law analysis of laminar flow in a channel filled with saturated porous media: a numerical solution. Entropy 2005;7(4):300-07.
[27] Nield DA. MODELLING FLUID FLOW IN SATURATED POROUS MEDIA AND AT INTERFACES. In: Ingham DB, Pop I, editors. Transport Phenomena in Porous Media II Oxford, Elsevier, 2002: 1-19.
[28] Nield DA. The Modeling of Viscous Dissipation in a Saturated Porous Medium. ASME- Journal of Heat Transfer 2007;in press.
[29] Hooman K. Comment on "Thermodynamics of natural convection in enclosures with viscous dissipation" in 48 (2005) 2333-2341 and "On natural convection in enclosures filled with fluid-saturated porous media including viscous dissipation" in 49 (2006) 2215-2226 by V.A.F. Costa. Int J Heat Mass Transf 2007;Submitted.
[30] Dagtekin I, Oztop H, Bahloul A. Entropy generation for natural convection in Γ-shaped enclosures. International Communications in Heat and Mass Transfer 2007;34:502-10.
[31] Hooman K, Gurgenci H, Merrikh AA. Heat transfer and entropy generation optimization of forced convection in porous-saturated ducts of rectangular cross-section. International Journal of Heat and Mass Transfer 2007;50(11-12):2051-59.
[32] Hooman K, Gurgenci H. Effects of viscous dissipation and boundary conditions on forced convection in a channel occupied by a saturated porous medium. Transp Porous Media 2007;68(3):301-19.
[33] Hooman K, Gurgenci H. Effects of temperature dependent viscosity on Bénard convection in a porous medium using a non-Darcy model. Int J Heat Mass Transf 2007;in press.
[34] Hooman K, Gurgenci H. Heatline visualization of natural convection in a porous cavity occupied by a fluid with temperature dependent viscosity. Journal of Heat Transfer-Transactions of the ASME 2008;in press.

Table 1 Comparison between <Ns> values predicted by Eq. (19) (in the parenthesis) and those obtained numerically.

h_1	Ra	Ω=0.02	Ω=0.04	Ω=0.06	Ω=0.08	Ω=0.1
0.25	10^3	3.655 (3.694)	3.586 (3.623)	3.52 (3.555)	3.457 (3.489)	3.395 (3.425)
	10^4	4.176 (4.248)	4.098 (4.166)	4.023 (4.088)	3.951 (4.012)	3.881 (3.939)
	10^5	6.537 (6.708)	6.416 (6.579)	6.3 (6.455)	6.188 (6.335)	6.079 (6.22)
0.5	10^3	4.086 (4.119)	4.009 (4.04)	3.935 (3.964)	3.864 (3.89)	3.796 (3.82)
	10^4	4.373 (4.424)	4.291 (4.339)	4.212 (4.257)	4.136 (4.178)	4.063 (4.102)
	10^5	6.701 (6.864)	6.576 (6.732)	6.457 (6.605)	6.342 (6.482)	6.231 (6.364)
0.75	10^3	3.69 (3.727)	3.621 (3.655)	3.555 (3.586)	3.49 (3.52)	3.428 (3.456)
	10^4	3.82 (3.857)	3.748 (3.782)	3.679 (3.711)	3.613 (3.642)	3.549 (3.576)
	10^5	5.115 (5.237)	5.02 (5.136)	4.929 (5.039)	4.841 (4.946)	4.756 (4.856)

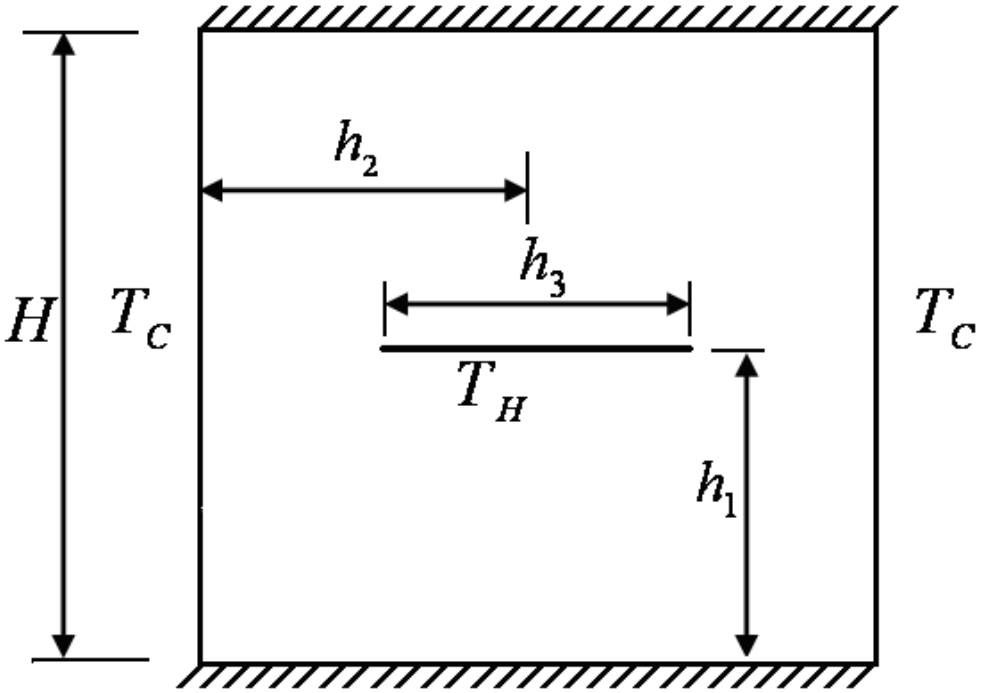

Fig.1. Definition sketch.

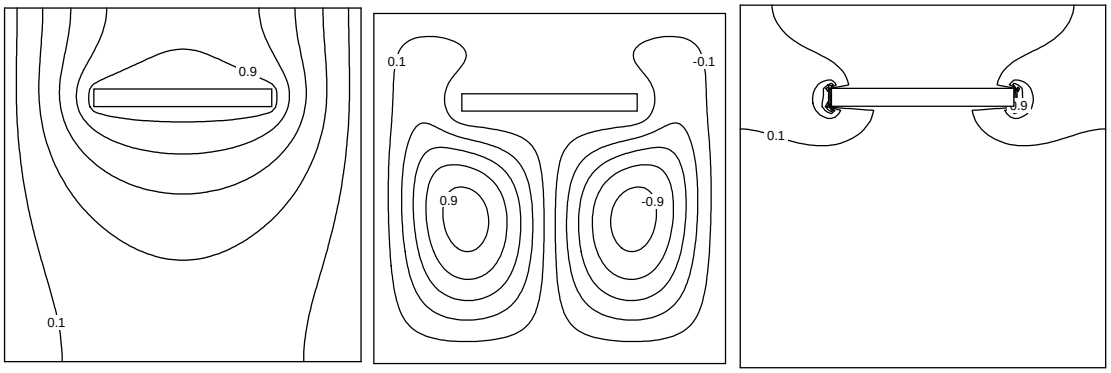

(a)

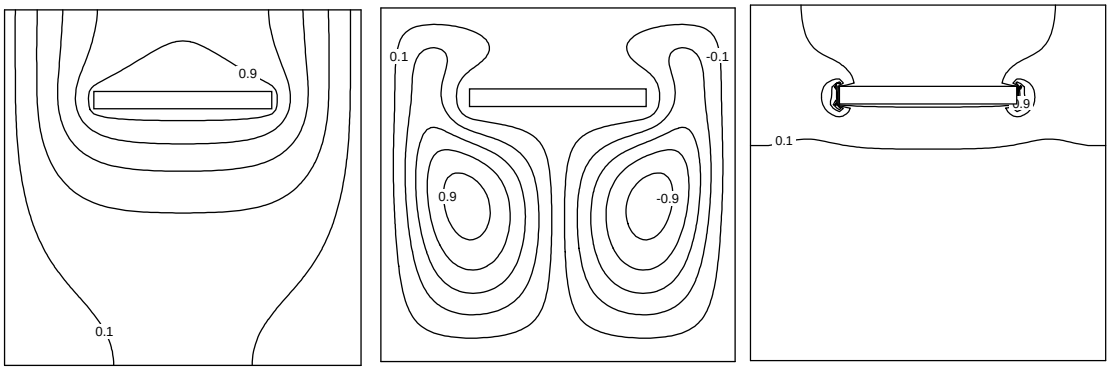

(b)

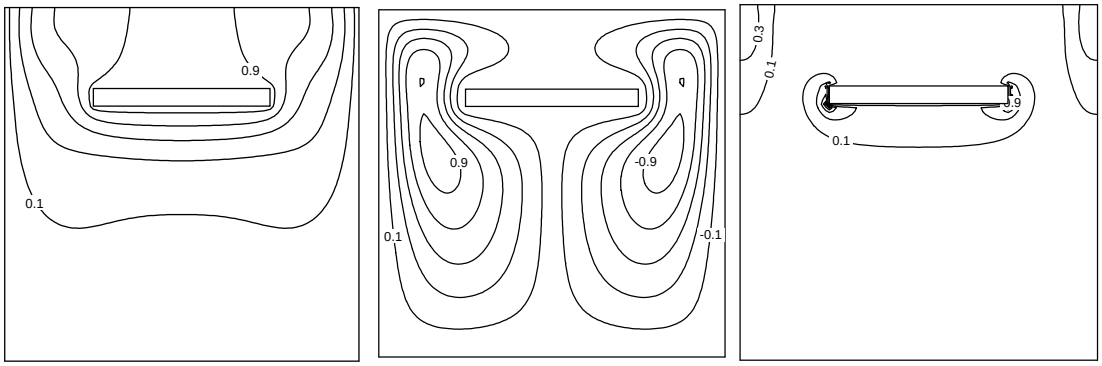

(c)

Fig. 2 Isotherms (left), streamlines (center), and dimensionless entropy generation rate (right) with h_1=0.75 for a) Ra=10^3, b)Ra=10^4, and c)Ra=10^5

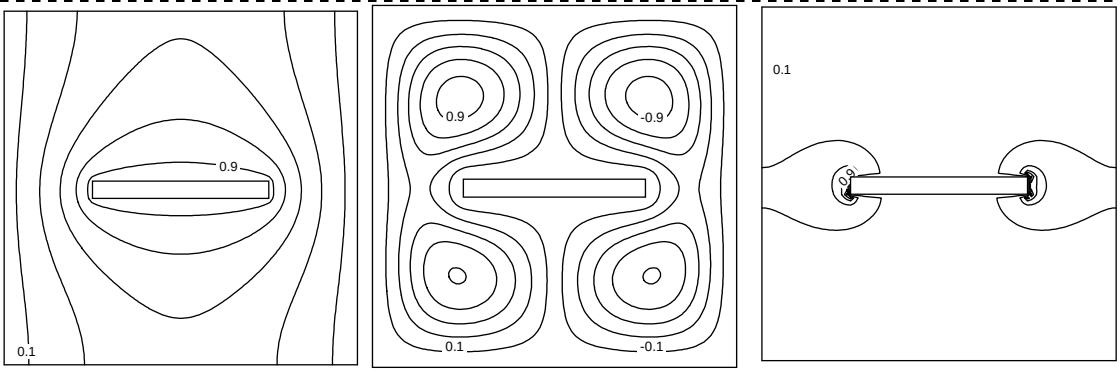

(a)

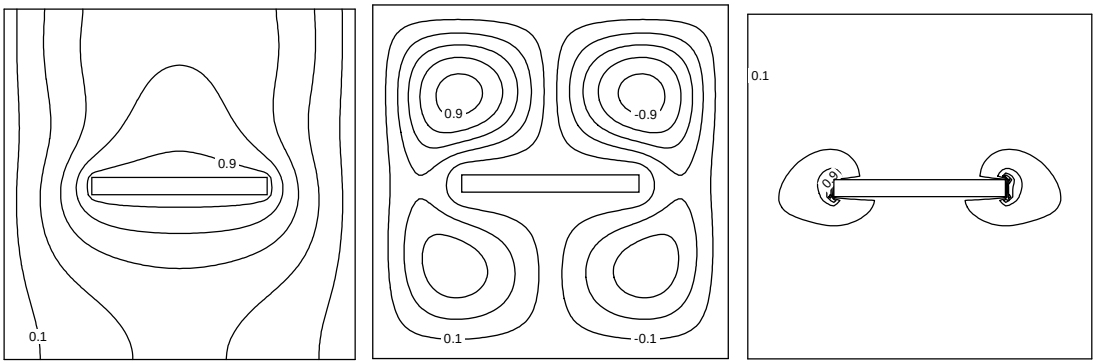

(b)

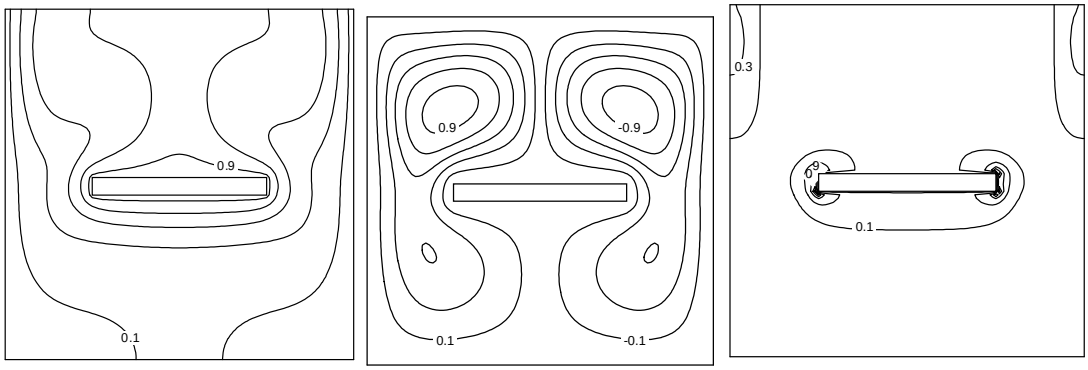

(c)

Fig. 3 Isotherms (left), streamlines (center), and dimensionless entropy generation rate (right) with h_1=0.5 for a) Ra=10^3, b)Ra=10^4, and c)Ra=10^5

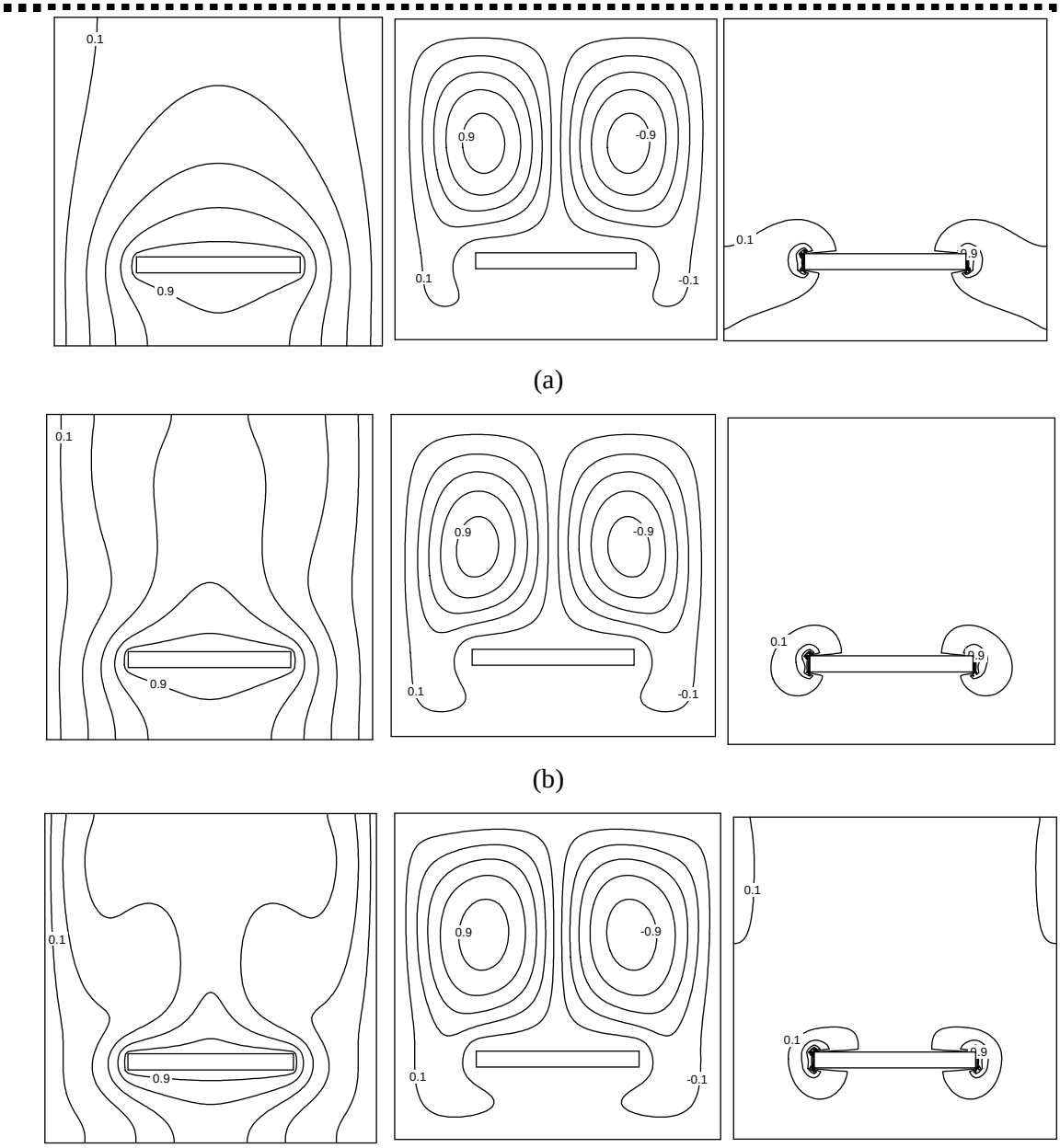

Fig. 4 Isotherms (left), streamlines (center), and dimensionless entropy generation rate (right) with h_1=0.25 for a) $Ra=10^3$, b)$Ra=10^4$, and c)$Ra=10^5$

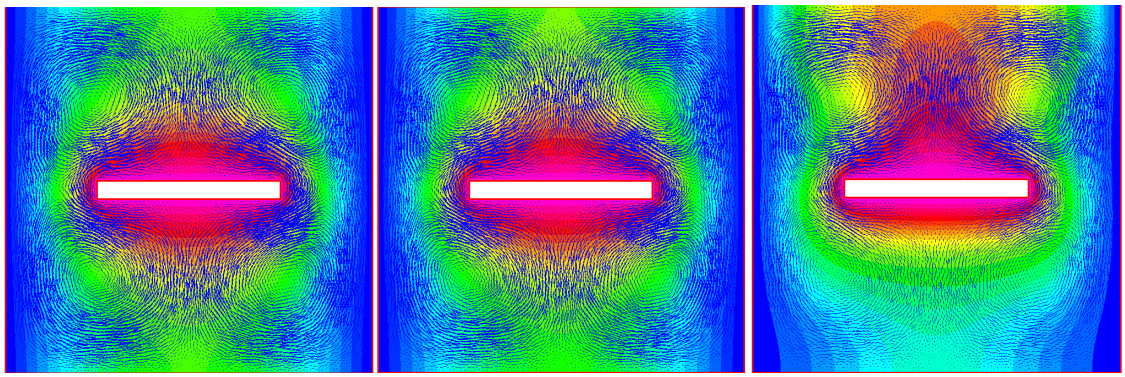

(a) (b) (c)

Fig. 5 Isotherms and velocity vectors with h_1=0.5 for a)Ra=10^3, b)Ra=10^4, and c)Ra=10^5

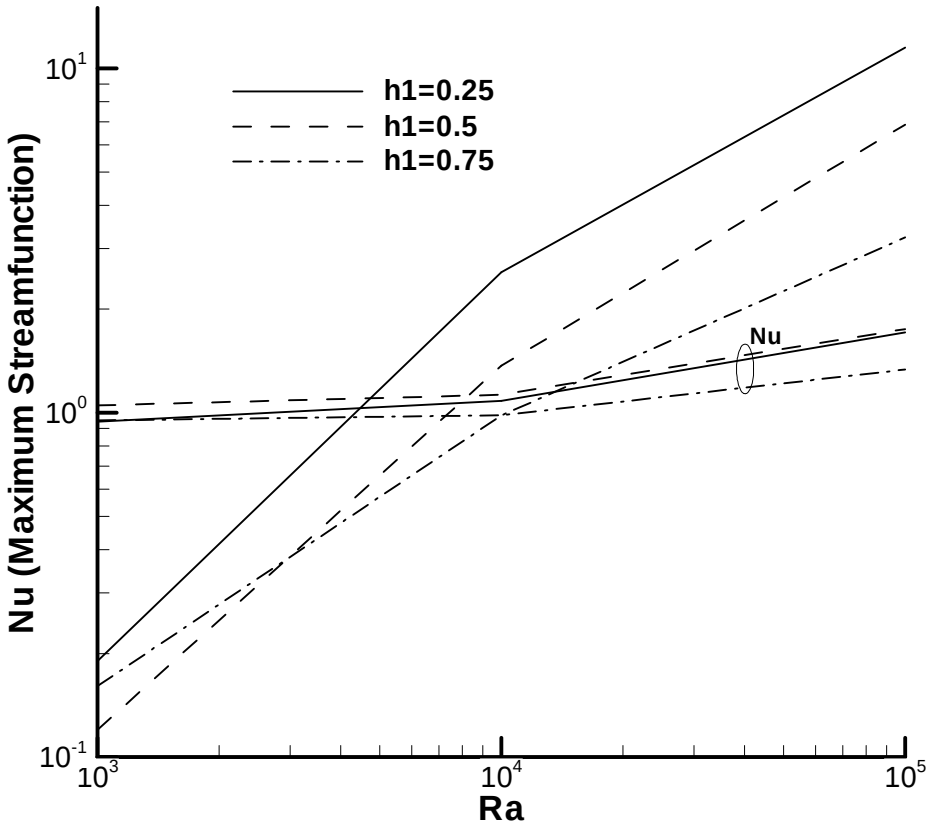

Fig. 6 Nu and ψ_{max} versus Ra for different plate positions

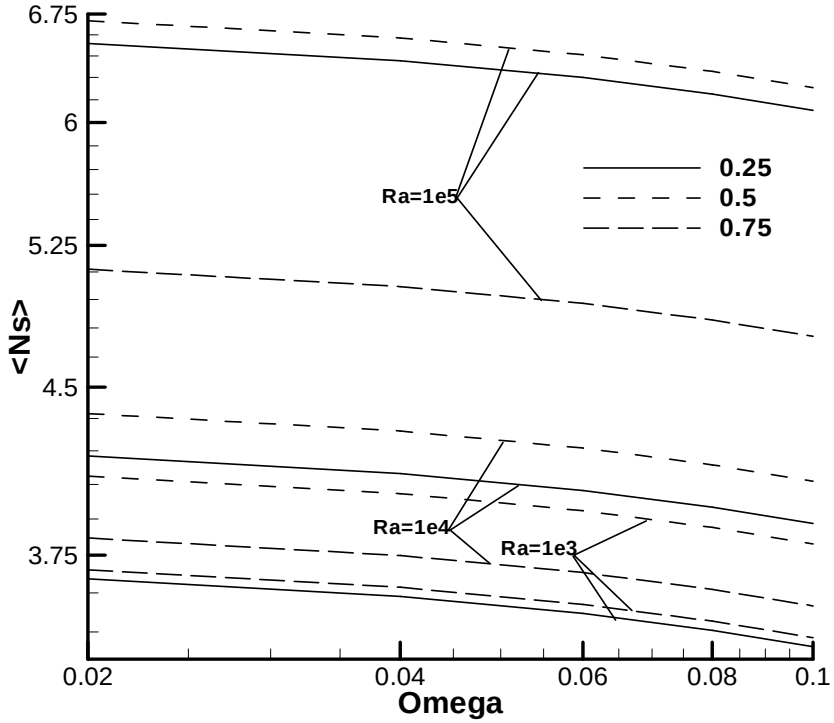

Fig. 7 Ns* versus Ω for different Ra values and plate positions